



## In-depth phenotypic characterization of reticulocyte maturation using mass cytometry

Richard Thomson-Luque<sup>a,1</sup>, Chengqi Wang<sup>a</sup>, Francis B. Ntumngia<sup>a</sup>, Shulin Xu<sup>a</sup>, Karoly Szekeres<sup>b</sup>, Amy Conway<sup>a</sup>, Swamy Rakesh Adapa<sup>a</sup>, Samantha J. Barnes<sup>a</sup>, John H. Adams<sup>a,\*</sup>, Rays H.Y. Jiang<sup>a,\*</sup>

<sup>a</sup> Center for Global Health and Infectious Diseases Research, College of Public Health, University of South Florida, Tampa, USA

<sup>b</sup> Department of Molecular Medicine, Morsani College of Medicine, University of South Florida, Tampa, USA

### ARTICLE INFO

#### Keywords:

Mass cytometry  
CyTOF  
Red blood cell  
Reticulocyte  
Maturation

### ABSTRACT

Progress towards an in-depth understanding of the final steps of the erythroid lineage development is paramount for many hematological diseases. We have characterized the final stages of reticulocyte maturation from bone marrow to peripheral blood using for the first time single-cell Mass Cytometry (CyTOF). We were able to measure the expression of 31 surface markers within a single red blood cell (RBC). We demonstrate the validity of CyTOF for RBC phenotyping by confirming the progressive reduction of transferrin receptor 1 (CD71) during reticulocyte maturation to mature RBC. We highlight the high-dimensional nature of mass cytometry data by correlating the expression of multiple proteins on individual RBCs. We further describe a more drastic reduction pattern for a component of the alpha4/beta1 integrin CD49d at the very early steps of reticulocyte maturation in bone marrow and directly linked with the mitochondria remnants clearance pattern. The enhanced and accurate RBC phenotyping potential of CyTOF described herein could be beneficial to decipher RBC preferences, as well as still not well understood receptor-ligand interaction of some hemotropic parasites such as the malaria causing agent *Plasmodium vivax*.

### 1. Introduction

Red blood cells (RBCs) are among the most uniform cell populations in the human body. The youngest RBCs in peripheral circulation, the reticulocytes, represent the endpoint of erythropoiesis in the bone marrow [1, 2]. To complete erythropoiesis, central macrophages in erythroblastic islands play instrumental roles providing iron, secreting cytokines, erythropoietin and transcription factors [3] and, very importantly, they perform phagocytosis of the protruding nuclei from the surrounding orthochromatic erythroblasts [4]. Junction maintenance of erythroblastic islands is via  $\alpha v$  integrins, VCAM-1 and EMP in macrophages interacting with ICAM-4, VLA-4 and EMP in erythroblasts [5, 6]. A complex number of molecules serves as intermediates in this process (CD151, CD81, CD82, CD44, CD98, CD147, CD163, CD169 and Siglec-1) [7–12]. Once enucleated, these cells become reticulocytes [13], which are released to the peripheral circulation to develop within 40 h [14] to fully mature RBCs. In conjunction with this developmental step, the reticulocyte membrane switches from an endocytic state [15] to a

preponderant exocytic status as RBCs mature in peripheral blood circulation. This leads in the reticulocyte-to-mature-RBC transition to a reduction of the surface membrane by expelling excess surface proteins [14]. Moreover, remnants of internal organelles such as ribosomes, endoplasmic reticulum (ER) and Golgi apparatus are also cleared, although their underlying mechanisms are not completely determined [16]. A macroautophagy pathway called mitophagy seems to be responsible for mitochondria degradation and clearance; yet, how early in reticulocyte maturation this is established is also not well understood.

Historically, the larger more amorphous reticulocytes [17] in peripheral circulation are also defined microscopically by their typical reticular network visible with supra-vital stains such as New Methylene Blue (NMB) and sub-classified in 4 Heilmeyer stages (I–IV) [18]. A classification for reticulocytes into R1, which would correspond to the more immature fraction of reticulocytes observed after enucleation in the bone marrow, and R2, located in peripheral blood, has been initially proposed [19]. However, nowadays RNA loss and above all the surface expression of CD71 are the most common markers used to define the

\* Corresponding authors at: Center for Global Health and Infectious Diseases Research, College of Public Health, University of South Florida, 3720 Spectrum Boulevard, Suite 304/404, Tampa, FL 33612-9415, USA.

E-mail addresses: [jadams3@health.usf.edu](mailto:jadams3@health.usf.edu) (J.H. Adams), [jiang2@health.usf.edu](mailto:jiang2@health.usf.edu) (R.H.Y. Jiang).

<sup>1</sup> Present address: Centre for Infectious Diseases, Parasitology, Heidelberg University Hospital, Im Neuenheimer Feld 324 (office & labs in INF 344), 69120 Heidelberg, Germany.

<https://doi.org/10.1016/j.bcmd.2018.06.004>

Received 7 May 2018; Received in revised form 24 June 2018; Accepted 24 June 2018

Available online 04 July 2018

1079-9796/© 2018 The Authors. Published by Elsevier Inc. This is an open access article under the CC BY-NC-ND license

(<http://creativecommons.org/licenses/by-nc-nd/4.0/>).

maturation from reticulocytes to fully mature RBCs [14]. Immature reticulocytes express higher levels of CD71 whereas during maturation, CD71 levels are reduced to barely measurable. Although composition, abundance, and changes in reticulocyte membrane proteins have been already studied during maturation [20–22], current single-cell studies based on flow cytometry have been limited to the number of spectrally resolvable fluorochromes [23].

Mass Cytometry (CyTOF) is the adaptation of Inductively Coupled Plasma Mass Spectrometry to single-cell analysis [14] and offers the ability to measure up to 40 parameters within a single cell [24–26]. This study is the first report to apply the powerful CyTOF phenotyping technology to characterize RBCs. Here, we bring a better understanding for the complexity of reticulocyte maturation from bone marrow to peripheral blood and suggest very immature reticulocyte surface molecules such as CD49d to be worth testing upon their role upon *Plasmodium vivax* (*P. vivax*) invasion mechanism.

## 2. Materials and method

### 2.1. Reticulocytes and mature RBCs

Four Duffy<sup>+</sup> (samples 1–4) and four Duffy<sup>−</sup> (samples 5–8) fresh reticulocyte and mature RBCs preparations (in total 8 peripheral blood samples) were obtained from Buffy coat (BC) packs (The Interstate Blood Bank INC, Memphis, USA). BC blood was centrifuged at 2500g for 5 min, washed with McCoy 5A incomplete Medium (MIM) (Sigma M4892-10L) and filtered for leuko-depletion on a NEO Purecell Leukocyte Reduction filter (Haemonetics). To separate reticulocytes from mature RBCs, we performed CD71 immuno-magnetic purification following the manufacturer's specifications (Miltenyi Biotec). CD71<sup>+</sup> and CD71<sup>−</sup> RBCs were separated on an autoMACS Pro Separator (Miltenyi Biotec), washed and re-suspended in MIM. NMB thin blood smears were performed after a 1:1 dilution and 15 min incubation at 37 °C to check for purity (generally above 95%). Reticulocytes and mature RBCs were kept at 4 °C in MIM until used, always before 2 days post isolation. One bone marrow reticulocyte preparation was obtained from unprocessed whole aspirates (ALLCELLS) following the same protocol as for peripheral blood BC packs, by which nucleated erythroblasts were retained in the Leukocyte Reduction filter. Residual WBC contamination (CD45<sup>+</sup> cells) was observed in our peripheral blood samples and slightly higher for bone marrow samples.

### 2.2. Mass cytometry

Commercially available metal-isotope-tagged antibodies against RBC surface markers were purchased from Fluidigm. When non-available, non-conjugated purified antibodies lacking carrier proteins were purchased from other companies (Table 1) and these antibodies were custom-conjugated by Fluidigm with heavy metal-preloaded maleimide-coupled MAXPAR chelating polymers (Table 1). A validation step was performed by Fluidigm to assure their viability (Supplemental Fig. 1). CD233 (Band 3) validation was not acceptable and therefore not taken into account for the ulterior analysis. CD234 (DARC) showed lower intensity signal than expected, yet it was acceptable for our purposes of distinguishing the different Duffy blood groups in our samples. In order to determine the differences in surface markers within maturation in RBCs we optimized the company's recommended protocol into a 3 days staining protocol for every sample. On day 1,  $1 \times 10^7$  mature RBCs or reticulocytes were re-suspended in PBS and Cell-IDTM Cisplatin (Fluidigm) to a final concentration of 5  $\mu$ M. The mixture was incubated at RT for 5 min followed by a quench staining with MaxPar Cell Staining Buffer (MCSB) (Fluidigm) using  $5 \times$  the volume of the cell suspension. For antibody staining, the RBC pellet was re-suspended in 50  $\mu$ L of MCSB. Then 50  $\mu$ L of metal isotopes labeled antibody cocktail prepared in MCSB, following the company's specifications, was added giving a total volume of 100  $\mu$ L. Samples were

vortexed, incubated for 30 min at RT and washed twice by adding 2 mL of MCSB, centrifuged and the supernatant discarded. We re-suspended our cells in 1 mL of a 0.05% glutaraldehyde solution (Sigma) and set at 4 °C for overnight shipment to The Human Immune Monitoring Center (HIMC), Stanford University, Palo Alto, California. Upon arrival on day 2, cells were centrifuged at 800g and washed twice with 1 mL of MCSB. The pellet was then incubated in 100  $\mu$ L of MaxPar Fix/perm Buffer at 4 °C for 30 min and then re-suspended in 1 mL Cell Intercalation Solution containing Cell-IDTM Intercalator-Ir (Fluidigm) to a final concentration of 125 nM, mixed and incubated overnight at RT. On day 3, cells were washed 2 times with 2 mL of MCSB and 2 more times with MilliQ water (Millipore). Prior to CyTOF run, pellet was adjusted to  $2.5\text{--}5 \times 10^5$ /mL. Data was acquired on a CyTOF 2 (Fluidigm) at HIMC. Data obtained by Mass Cytometry was converted to a FCS file and analyzed by FlowJo software (Treestar Inc.). We first gated out EQ-beads used for internal compensation. We set  $10^1$  as a threshold for negativity/background using BIP (a *Plasmodium* spp. specific C-terminal peptide epitope involved in endoplasmic reticulum retrograde trafficking) that should not be expressed on human RBCs. Using this  $10^1$  threshold, we gated out CD45<sup>+</sup> cells to skip analyzing any remnants of white blood cells post leuko-depletion. We were able to fully analyze 43,465 to 234,004 events per sample. For every RBC marker, we determined the positive and the negative population based on the  $10^1$  set threshold for negativity. Moreover, for every RBC marker, either positive or negatively expressed, we determined the expression of the whole set of markers to determine their correlation (i.e. CD41<sup>+</sup>-CD49d<sup>+</sup>/CD41<sup>+</sup>-CD49d<sup>−</sup>/CD41<sup>−</sup>-CD49d<sup>+</sup>/CD41<sup>−</sup>-CD49d<sup>−</sup>).

### 2.3. Computational methods and statistical analysis

#### 2.3.1. Generation of a marker intensity matrix

In order to represent and analyze the data obtained by mass cytometry regarding the intensity of 31 RBC markers for each single cell in sample  $s$  ( $s \leq 12$ ,  $s \in N1\text{--}N4$ ,  $R1\text{--}R8$ ) we generated a matrix  $M_{ij}^s$ , where  $i$  indicates each single cell in specific samples ( $i \leq$  the total number of cells in sample  $s$ ); and  $j$  indicates the specific RBC marker ( $1 \leq j \leq 31$ ).

#### 2.3.2. RBC markers correlation between different RBCs type

For each sample  $s$ , we calculated the number of cells  $N_j$  with specific marker  $j$ . It can be represented as:

$$N_j = \sum_i 1(M_{i,j} > 10)$$

here,  $1$  represents the indicator function. Thus, we have a vector ( $N_1^s, N_2^s, N_3^s, \dots, N_{31}^s$ ) to represent each sample  $s$ . The Pearson correlation can be calculated for each pair of samples.

#### 2.3.3. CD71 marker threshold selection

For mass cytometry analysis, reticulocytes from R1–R4 samples were classified in 2 groups based upon CD71 intensity for peripheral blood ( $< 400$  &  $> 400$ ). We choose this cut-off based on the estimated background signal obtained in fully mature RBCs. The quantile distribution of the CD71 intensity in mature RBCs is 4.69 for 0%, 23.18 for 25%, 45.47 for 50%, 99.32 for 75% and 381.33 for 100%. Since the biggest CD71 in N cell was  $\sim 382$ , we choose 400. With the threshold 400, over 99.9999% cells show non-significant CD71 levels.

#### 2.3.4. Visualization of multiple single-cell data sets

We used the cloud-based platform Cytobank ([www.cytobank.org](http://www.cytobank.org)), for analysis and visualization of multiple single-cell data sets simultaneously. We used SPADE (spanning-tree progression analysis for density-normalized events) to cluster over 100,000 sets of single-erythroid data into phenotypically similar cells of hierarchical trees.

**Table 1**

Antibodies, clones, metal isotopes tagged antibodies and companies used for flow cytometry and mass cytometry analysis. Commercially available metal isotopes tagged antibodies were purchased from Fluidigm. Other antibodies were purchased from other companies and custom-conjugated with heavy metal-preloaded maleimide-coupled MAXPAR chelating polymers by Fluidigm. Targets are termed by their cluster of differentiation (CD) and alternative names. Custom-conjugated antibodies went through an extra validation process by Fluidigm (\*) (Supplemental Fig. 1).

Target name	Target alternative names	Clone	Ab company	Metal isotope conjugation	Custom validation
CD71	Transferrin receptor	OKT-9	Fluidigm	168Er	
CD58 (LFA-3)	Lymphocyte function-associated antigen 3 (LFA-3)	TS2/9	Fluidigm	176Yb	
CD49f	Integrin alpha.6 (ITGA6)	G0H3	Fluidigm	164Dy	
CD81	Target of the antiproliferative antibody/tetraspanin-28	5A6	Fluidigm	145Nd	
CD41	Integrin alpha-IIb (ITGA2B)	HIP8	Fluidigm	89Y	
CD235ab	Glycophorin A/B	HIR2	Fluidigm	171Yb	
CD44	Hermes antigen/homing cell adhesion molecule (HCAM)	IM7	Fluidigm	156Gd	
CD147	Basigin (BSG)	HIM6	Fluidigm	170Er	
CD99	MIC2/single-chain type-1 glycoprotein	HCD99	Fluidigm	148Nd	
CD55	Complement decay-accelerating factor (DAF)	JS11	Fluidigm	160Gd	
CD49e	Integrin alpha-5 (ITGA5)	NKI-SAM-1	Fluidigm	161Dy	
CD49b	Integrin alpha-2 (ITGA2)	P1E6-C5	Fluidigm	141Pr	
CD49d	Integrin alpha-4 (ITGA4)	9F10	Fluidigm	163Dy	
CD49a	Integrin alpha-1 (ITGA1)	TS2/7	Fluidigm	152Sm	
CD36	Platelet glycoprotein 4/fatty acid translocase (FAT)	5-271	Fluidigm	154Sm	
CD45	Leukocyte common antigen (LCA)	HI30	Fluidigm	144Nd	
CD15	3-FAL, ELAM 1 ligand, fucosyltransferase, Leu M1	W6D3	Fluidigm	143Nd	
CD98	Large neutral amino acid transporter (LAT1)	UM7F8	Fluidigm	159Tb	
CD163	M130	GHI/61	Fluidigm	165Ho	
CD111	Nectin-1/poliiovirus receptor-related 1 (PVRL1)	R1.302	Biologend	172Yb	*
CD106	Vascular cell adhesion protein 1 (VCAM-1)	VCMA-1	Biologend	147Sm	
CD49c	Integrin alpha-3 (ITGA3)	GoH3	Biologend	149Sm	*
CD51/61	Integrin alpha-V (ITGAV)	23C6	Biologend	150Nd	*
CD47	Integrin associated protein (IAP)	B6H12	Biologend	166Er	*
CD82	KAI1, tetraspanin-27	ASL-24	Biologend	158Gd	*
CD151	Raph blood group	50-6	Biologend	142Nd	*
CD236	Glycophorin C	RET401	ThermoFisher	169Tm	
CD238	Kell antigen system	BRIC203	ThermoFisher	155Gd	*
CD242	Intercellular adhesion molecule-4 (ICAM4)/Landsteiner and Wiener blood system	polyclonal	R&D Systems	153Eu	*
CD234	Duffy antigen/chemokine receptor (DARC)	REA376	R&D Systems	146Nd	*
EMP/MAEA	Erythroblast macrophage protein/macrophage erythroblast attacher	polyclonal	R&D Systems	173Yb	
CD235b	Glycophorin A/MNS blood group	polyclonal	US Biological	169Tm	
BIP	<i>Plasmodium</i> spp. specific C-terminal peptide epitope involved in endoplasmic reticulum retrograde trafficking	Polyclonal	In house production	151Eu	

## 2.4. FACS sorting

$1 \times 10^9$  CD71<sup>+</sup> BC reticulocytes were incubated with anti-human CD71 and sorted into 3 different populations (CD71<sup>low</sup>, CD71<sup>med</sup> and CD71<sup>hi</sup>) on a BD FACS Aria II. Flow rate for cell sorting was set at 10,000 events/s on a purity mode. All sorting was performed with the sample placed on a pre-cooled chamber at 4 °C to avoid room temperature (RT) maturation and subsequent maturation and loss of CD71 on reticulocytes. We confirmed the correct FACS sorting by performing NMB staining and Immunofluorescence (IFA).

## 2.5. Immunofluorescence

To further validate FACS sorting we determined the different CD71 intensity in CD71<sup>low</sup>, CD71<sup>med</sup> and CD71<sup>hi</sup> FACS-sorted reticulocytes by IFAs. CD71<sup>low</sup>, CD71<sup>med</sup> and CD71<sup>hi</sup> FACS-sorted reticulocytes were washed with PBS-0.05% BSA and incubated with CD71 FITC (BD) for 30 min at 4 °C; after incubation cells were washed twice with PBS-0.05% BSA and smeared. Images were obtained in an Operetta platform (Perkin Elmer) at 60 $\times$ .

To visualize enucleation on HSC cultures, HSC-derived cultured cells were washed with PBS-0.05% BSA, re-suspended in PBS-0.05% BSA and then stained with anti-human CD71-FITC and DAPI (4,6 diamidino-2-phenylindole) (Life technologies) for 30 min at 4 °C. Cells were then washed twice with PBS-0.05% BSA, smeared on a glass slide and acquired in an Operetta platform at 60 $\times$ .

## 2.6. Hematopoietic stem cells (HSC) cultures

CD34<sup>+</sup> cells were isolated from peripheral blood mononuclear cells (PBMC) (The Interstate blood bank). PBMC were separated by Ficoll-Isopaque (GE Healthcare) density gradient. Briefly, 40 mL of blood was diluted 1:1 with Hanks Balanced Salt Solution (HBSS) containing 0.6% (v/v) ACD and centrifuged at 400g for 30 min at RT without break. After washing the pellet twice, AKT (Gibco) lysis was performed for 10 min at RT, followed by two rounds of washes with HBSS. CD34<sup>+</sup> isolated cells were then re-suspended in 10 mL cold autoMACS running buffer (Miltenyi Biotech) before proceeding to immune-magnetic purification in an autoMACS Pro Separator (Miltenyi Biotech) on positive selection mode according to the company's recommended procedure. Then we proceeded to expanding the number of cells in vitro using T25cm<sup>2</sup> tissue culture flasks (Thermo Fisher Scientific) at 37 °C with 5% CO<sub>2</sub>. 4 mL Glutamax-Isocove modified media (IMDM) (Biochrom) per flask was supplemented with 5% human AB serum, 1% Penicillin/Streptomycin (v/v) (Invitrogen), Inositol (40  $\mu$ g/mL, Sigma), Folic acid (10  $\mu$ g/mL, Sigma), Monothioglycerol (1.6  $10^{-4}$  M, Sigma), Holotransferrin (200  $\mu$ g/mL, Sigma), Heparin 3 U/mL and insulin from bovine pancreas (10  $\mu$ g/mL, Sigma). From day 0 to 8, CD34<sup>+</sup> cells were cultured with Stem Cell Factor (SCF, 40  $\mu$ g/mL, Bioke), IL-3 (1 ng/mL, R&D System), Hydrocortisone (HDS,  $10^{-6}$  M, Sigma), and Erythropoietin (EPO, 3 IU/mL, R&D System). Flasks were split whenever the total number of cells per flask was over  $1 \times 10^6$ /flask during the whole process of expansion. At day 8, IMDM medium was depleted of IL-3 and Holotransferrin was increased to 1 mg/mL. After day 11 we

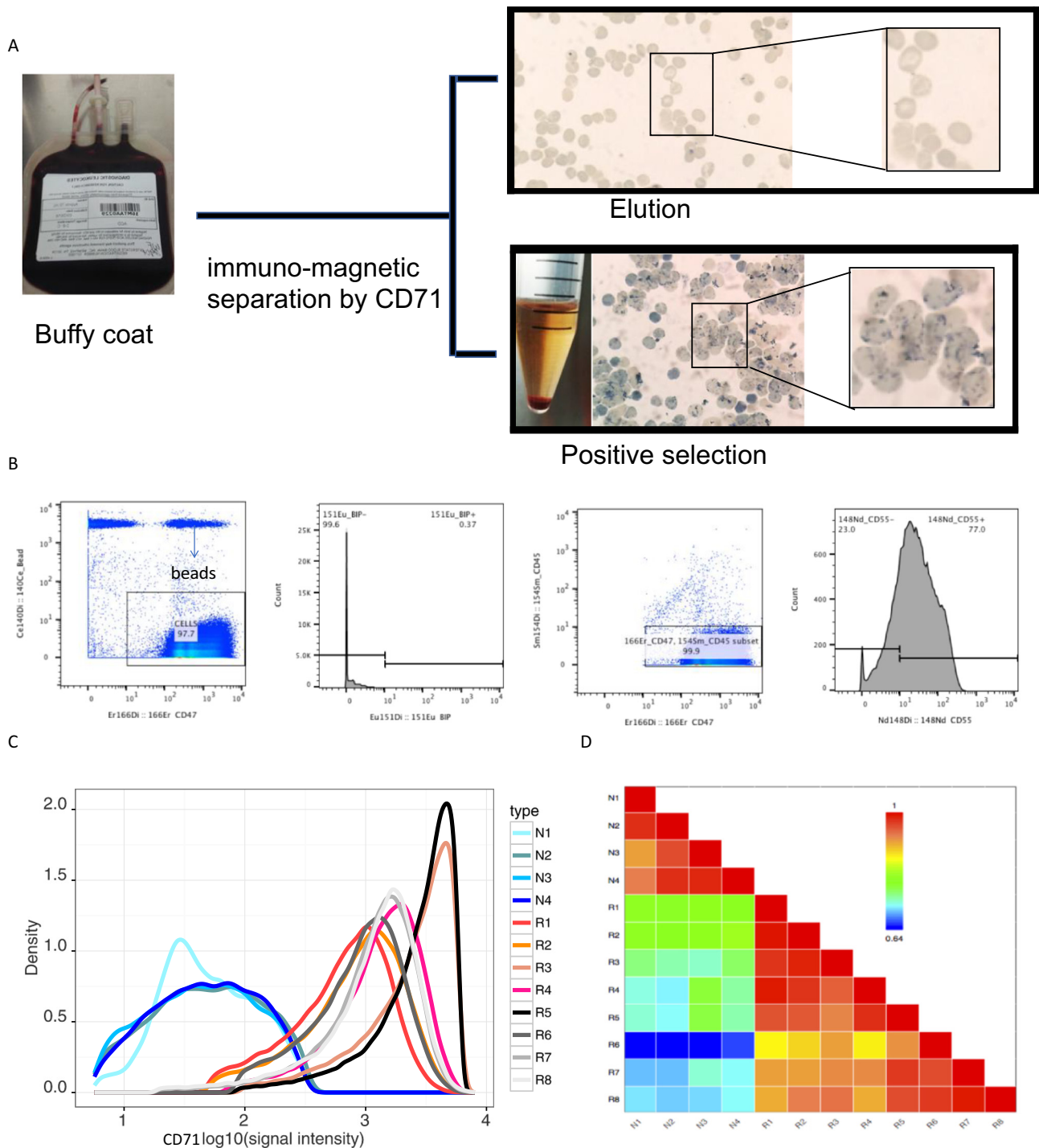


**Fig. 1.** Initial validation of samples. (A) NMB staining confirmed a distinct inner reticulae pattern present in > 95% of immune-magnetically isolated CD71<sup>+</sup> reticulocytes, while marginal or absent from CD71<sup>-</sup> cells (mature RBCs). (B) Gating strategy. We first excluded EQbeads used as internal compensation. As a threshold for negativity we established 10<sup>1</sup>, representing the level above which no signal was found for the non-human RBC marker BIP. To skip confounding results from marginal contamination with WBCs, CD45<sup>+</sup> cells were excluded from the analysis. Finally, for every RBC marker, the positive and negative cells for every sample were inferred as shown in the example for CD55. (C) Histogram plot showing the different CD71 intensities in Duffy<sup>+</sup> mature RBCs (N1–N4), Duffy<sup>+</sup> reticulocytes (R1–R4) and Duffy<sup>-</sup> reticulocytes (R5–R8). Inter-sample variability in CD71 expression between R1–R8 reflects inter-human heterogeneity and reinforces our analysis. (D) Heat map comparing for all samples (R1–R8 and N1–N4) the correlation of the whole set of RBC markers studies by CyTOF in a color scale from 0.64 (low) to 1 (very high): high correlation between Duffy<sup>+</sup> mature RBCs (N1–N4); high correlation between all Duffy<sup>+</sup> reticulocytes samples (R1–R4); high correlation between all Duffy<sup>-</sup> reticulocytes samples (R5–R8); lower correlation between N1–N4 and R1–R4; low correlation between N1–N4 and R5–R8; moderate correlation between R1–R4 and R5–R8.

depleted the IMDM medium of SCF but it still contained EPO (3 IU/mL) until the end of the culture at day 18. Cells were then stained with Trypan Blue solution 0.4% (Sigma) for estimation of cell death and counted daily on a Neubauer chamber. The morphology and percentage of enucleation at days 14, 15, 16, 17 and 18 were tracked on independent *in vitro* cultures ( $n = 8$ ) (except at day 17 with  $n = 5$ ) by cytospin centrifugation at 200g for 5 min and 1000 cells counts on Giemsa stained smears. To further visualize enucleation on HSC cultures, HSC-derived cultured cells were washed with PBS-0.05% BSA, re-suspended in PBS-0.05% BSA and then stained with anti-human CD71-FITC and DAPI (4,6 diamidino-2-phenylindole) (Life technologies) for 30 min at 4 °C. Cells were then washed twice with PBS-0.05% BSA, smeared on a glass slide and acquired in an Operetta platform at 60 $\times$ . HSC derived reticulocytes from independent cultures ( $n = 3$ ) at days 14 and 15 were filtered on a NEO Purecell Leukocyte Reduction filter for the assessment of their CD49d, CD36 and CD44 expression before and after filtration by flow cytometry.

### 2.7. Flow cytometry

For flow cytometry phenotypic analysis of HSC-derived cells before and after filtration,  $5 \times 10^5$  HSC-derived cells were washed in PBS/0.05% BSA, re-suspended in 100  $\mu$ L of Brilliant Stain Buffer (BD Horizon) and stained for 30 min at 4 °C with the following anti-human antibodies: anti-CD49d-PE (Miltenyi), anti CD36-APC and anti-CD44-APC (Biolegend). Cells were washed twice with PBS/0.05% BSA and over 50,000 events were recorded BD Accuri C6 flow cytometer (BD Biosciences-US). Analysis was performed on a BD FACSDiva v6 Software.

### 2.8. High content imaging

To quantify the mitochondria content of different subpopulation reticulocytes (CD71<sup>low</sup>, CD71<sup>med</sup> and CD71<sup>hi</sup> reticulocytes) obtained by of FACS-sorting, High Content Imaging (HCI) was applied. Images were acquired in an Operetta platform (Perkin Elmer). A micro-engineered Micro-Well Device (MWDs) was fabricated by the Draper Lab. Two molded PDMS layers are bonded to a No.1 glass cover slip, the top containing eight independent macro-scale wells of 10 mm in diameter and 5 mm deep each. The next PDMS layer contains arrays of molded micro-wells that are 100  $\mu$ m in diameter and 100  $\mu$ m deep. Nine hundred microwells align underneath each macro-scale well. Reticulocytes were incubated with anti-human CD71-APC and Mitotracker-Orange for 30 min at 4 °C; after incubation cells were washed twice with PBS and loaded into the well with 200  $\mu$ L of diluted reticulocytes in PBS/0.1% BSA at a 0.025% hematocrit, with an average 55.5 RBCs/micro-well, by pipetting up and down gently. Cells were spun down at 50g with acceleration 6 and deceleration 6 for 3 min at RT in a homemade black MWD centrifuge box on a Sorvall RC6+ centrifuge (Thermo Scientific) with the 96-well plate rotor adaptor to push the cells off the walls of the microwells. Images were obtained following this protocol: MWDs were scanned with brightfield at 2 $\times$  objective at exposure time of 5 ms and 2  $\mu$ m height, to serve as the background for fields of view selection. Then 60 $\times$  objective Z-stacks of 0.5  $\mu$ m at exposure time of 200 ms were taken to set up the best height for quality images. We set a very restrictive algorithm to account a cell as being mitochondria<sup>+</sup> (ratio spots > 2/spots > 0). We are aware that by applying such a conservative algorithm we might have underestimated the amount of real inner reticulocyte mitochondria content. Notwithstanding, we preferred this scenario as we assumed that these same restrictions would be shared among the different CD71 populations and besides we would skip background.

## 3. Results

### 3.1. Mass cytometry: 31 markers within a single RBC

This study uses novel the novel mass cytometry/CyTOF technology to characterize single-cell phenotypes of reticulocytes and mature RBCs from bone marrow to peripheral blood. The current CyTOF methodology for peripheral blood mononuclear cells (PBMCs) was adapted to characterize single RBCs. We used metal-isotope-conjugated antibodies against 31 validated RBC membrane proteins (Table 1 and Supplemental Fig. 1) for analysis of eight healthy donors, four Duffy<sup>+</sup> (1–4) and four Duffy<sup>−</sup> (5–8). Prior to analysis, reticulocytes (R1–R8) were separated from mature RBCs (N1–N4) by CD71 immune-magnetic labeling (Fig. 1A) and stained with new methylene blue (NMB). This traditional staining method to define reticulocytes confirmed the CD71<sup>+</sup> cells were rich in reticular network in > 95%, while CD71<sup>−</sup> mostly corresponded to mature RBCs almost lacking such internal structures and confirming a good isolation efficiency. Yet, we were sometimes able to detect marginal levels of CD71 (although 100 times lower than reticulocytes) in some mature RBCs attributed to minor reticulocyte contamination in the N samples as also referred by others [27].

For CyTOF background signal control during RBCs gating strategy (Fig. 1B), we used BIP, a *Plasmodium* spp. specific C-terminal peptide epitope involved in endoplasmic reticulum retrograde trafficking. BIP is absent in human RBCs and was used as a negative control to set the detection threshold of 10<sup>1</sup>. Importantly, the reactivity of all 31 antibody markers showed very high reproducibility in biological replicates between donors. Indeed, reticulocytes and mature RBCs within an individual were more different than reticulocytes between donors, as shown with lower level of CyTOF signal correlations of markers between N1–N4 compared to R1–R8 (Fig. 1C–D). The intercellular heterogeneity of CD71 in the samples reflects the different maturation state of the whole subset of reticulocyte within an individual sample based on the internalization and later sorting of the transferrin receptor via the exosomal pathway.

### 3.2. The current CD71 reticulocyte maturation model is captured by mass cytometry

To better understand reticulocyte maturation, we used CyTOF to compare expression levels of 31 RBC markers in reticulocyte maturation stages based on CD71 intensity. We classified reticulocytes from R1–R4 samples in 2 groups based upon CD71 intensity for peripheral blood (< 400 & > 400). We then compared both reticulocyte groups to mature RBCs from N1–N4 samples, in a total of 500,000 single cells (Fig. 2). In this initial CyTOF analysis the pattern of differences for our diverse set of RBC markers was consistent with the expected CD71-based maturation model. For the RBC maturation process, CyTOF results on single-cell reticulocytes showed a progressive decreased ( $p < 0.001$ ) levels of CD36, as expected, as well as for CD98, CD44, CD151, CD81 and CD82. In contrast, a significantly and more accentuated decreased ( $p < 0.001$ ) levels of CD49d was found between cells with higher and lower surface expression levels of CD71 (< 400 & > 400) (Fig. 2). We next investigated whether peripheral blood reticulocytes might still retain some of their macrophage-interacting proteins, such as CD51–61, CD106, CD163 and EMP-Maea, together with other erythroblast counterparts such as CD99 and CD242. Our results show that peripheral blood reticulocytes do not appear to retain their macrophage interacting proteins, as only minimal levels of expression of EMP-Maea and CD51–61 could be detected (Fig. 2). Moreover, even in the most immature reticulocytes (CD71 > 400), very low levels of CD106 and CD163 are present (Fig. 2). An overall surface similarity with no significant differences was observed when we compared between Duffy<sup>+</sup> and Duffy<sup>−</sup> reticulocytes (Supplemental Fig. 2).

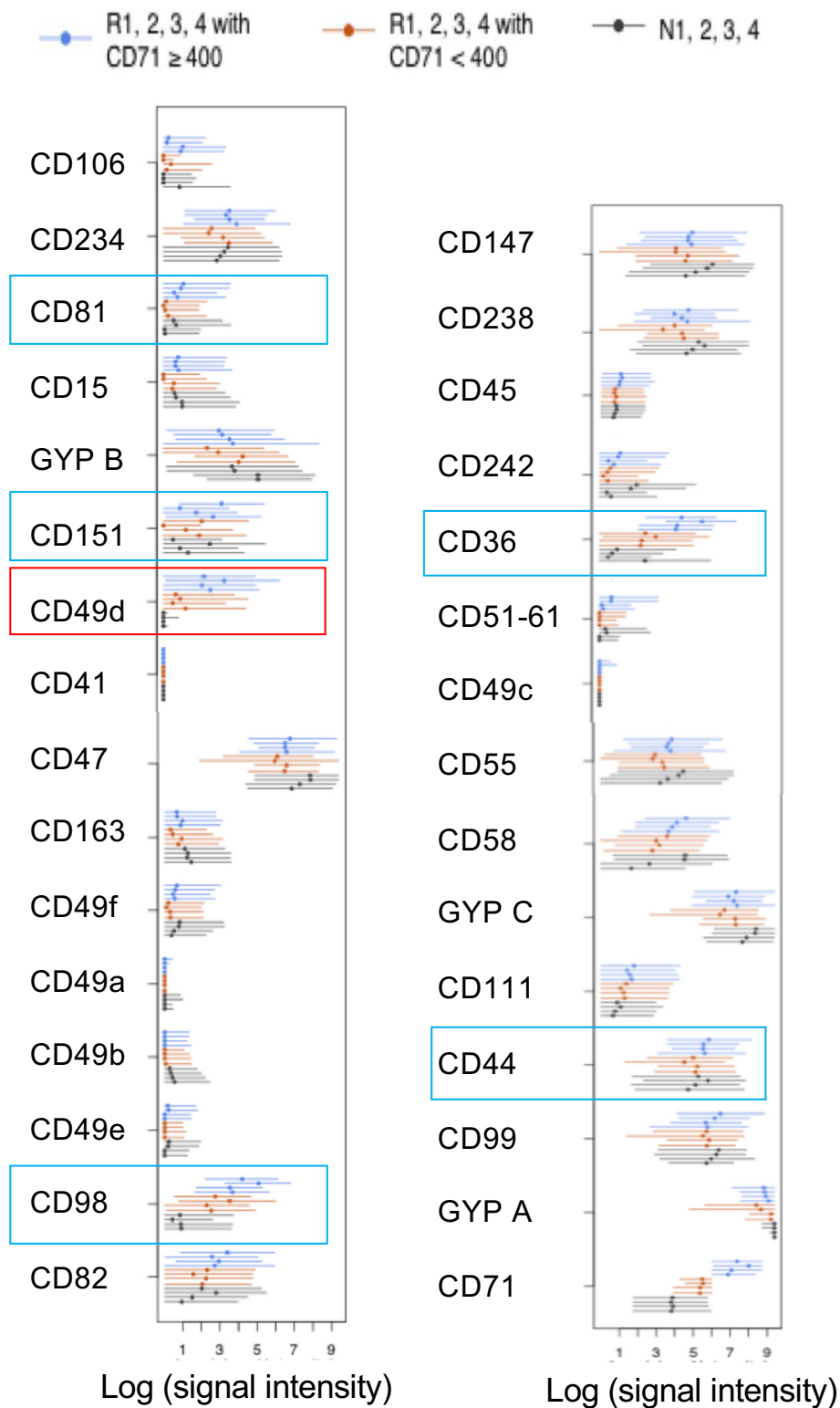
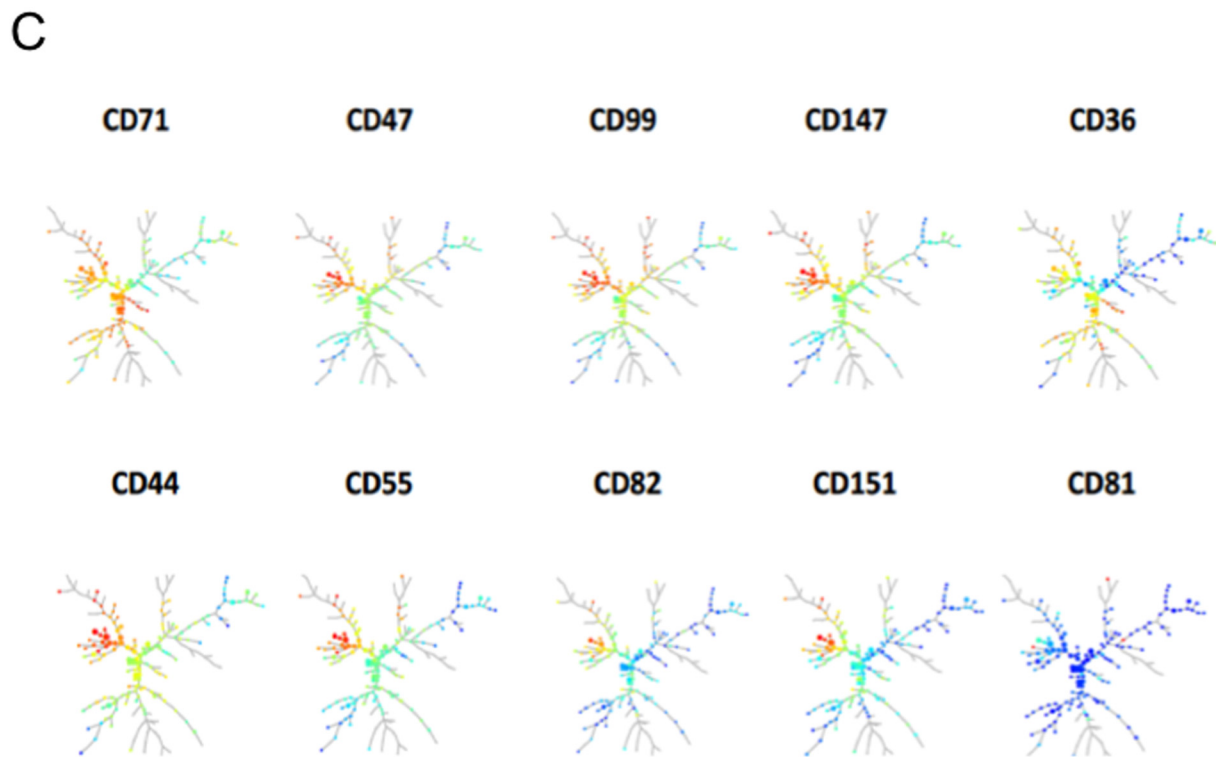
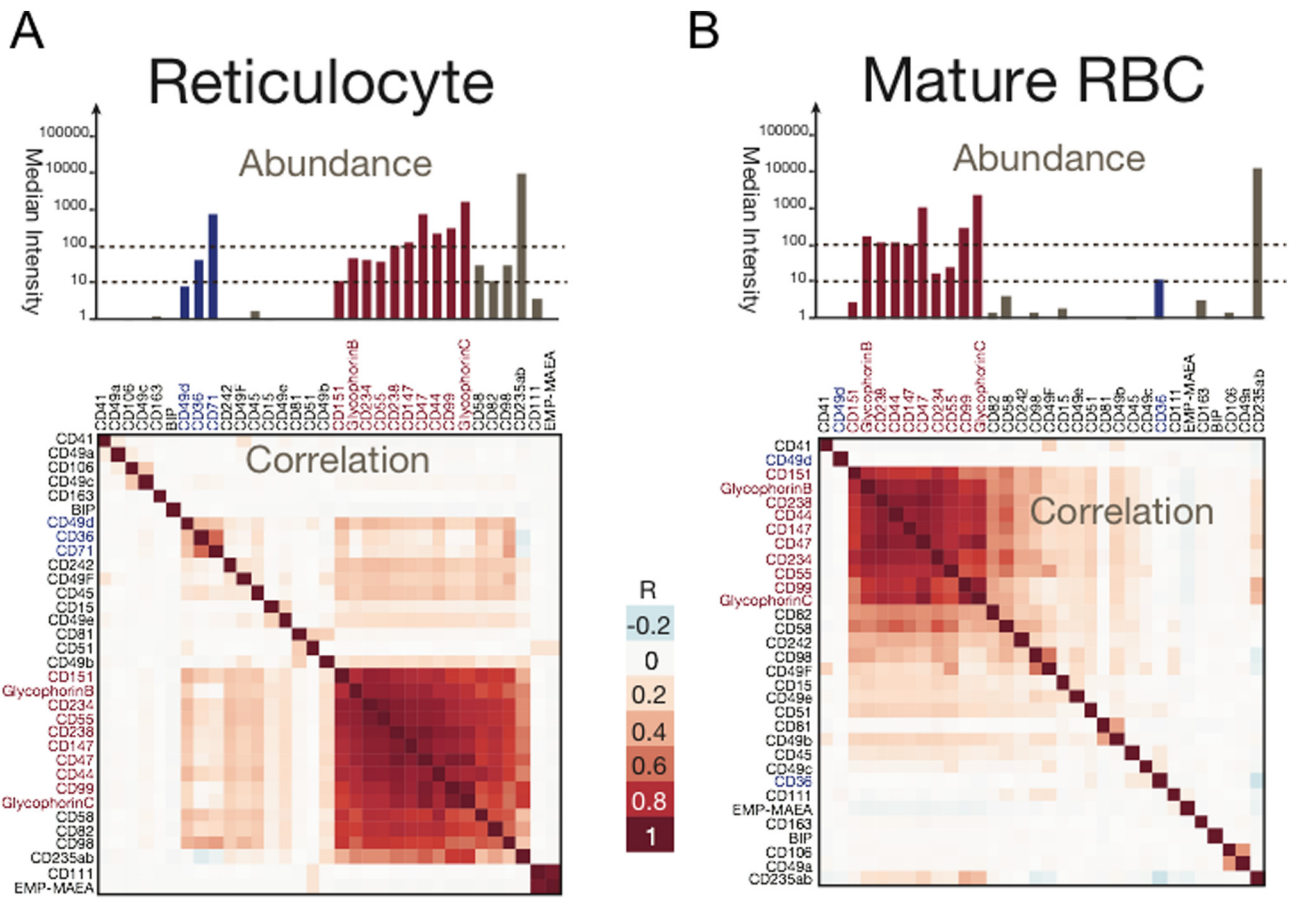


Fig. 2. Signal intensities (log scale) of all RBCs markers determined by CyTOF in peripheral blood. (A) Differential markers intensity within 4 mature RBCs Duffy<sup>+</sup> samples (N1–N4) and 4 reticulocyte Duffy<sup>+</sup> samples (R1–R4), separated by levels of CD71 intensity (< 400 & > 400), from peripheral blood from the same donor. Blue boxes represent markers with high variability on intensity during maturation; red box calls for the highest variability on intensity during maturation for CD49d. (For interpretation of the references to color in this figure legend, the reader is referred to the web version of this article.)

### 3.3. Reticulocyte markers follow distinct patterns of disappearance during maturation

The high-dimensional nature of mass cytometry data and CYTOF capability to study the expression of > 30 markers enables

simultaneous analysis of multiple proteins on individual cells (Fig. 3). We observe that a cluster of immature RBC markers follows a faster decreasing pattern as reticulocytes progress to mature RBCs (Fig. 3A). Combinatorial analysis of the expression of these markers showed a correlation among themselves in the reticulocyte population (Pearson's



(caption on next page)

**Fig. 3.** Multidimensional analysis. (A–B) Correlation and abundance of RBC markers in reticulocytes and mature RBCs. A group of markers (CD55, CD238, CD44, CD47, CD147, CD234, CD99, CD58 and CD151) with high median intensity (dark red) are highly correlated among themselves (Pearson's  $r > 0.8$ ) and present a smooth decreasing pattern of expression from reticulocytes to mature RBC. The expression of mature RBC markers GYPA, GYPB and GYPC also with high median intensity (dark red) increases as expected. Immature markers (CD49d, CD49f and CD242) (dark blue and light blue) form a separate correlation cluster (Pearson's  $r > 0.8$ ) showing a pronounced decrease in expression during maturation. The expression and correlation of the highly expressed markers (dark red) in reticulocytes is persistent in mature RBCs; conversely the cluster of immature markers found in reticulocytes is absent. (C) Multidimensional analysis using Spanning-tree Progression Analysis of Density-normalized Events (SPADE). Clustering phenotypically similar cells in hierarchical trees analysis shows non-uniformity in the expression of RBC markers in reticulocytes. (For interpretation of the references to color in this figure legend, the reader is referred to the web version of this article.)

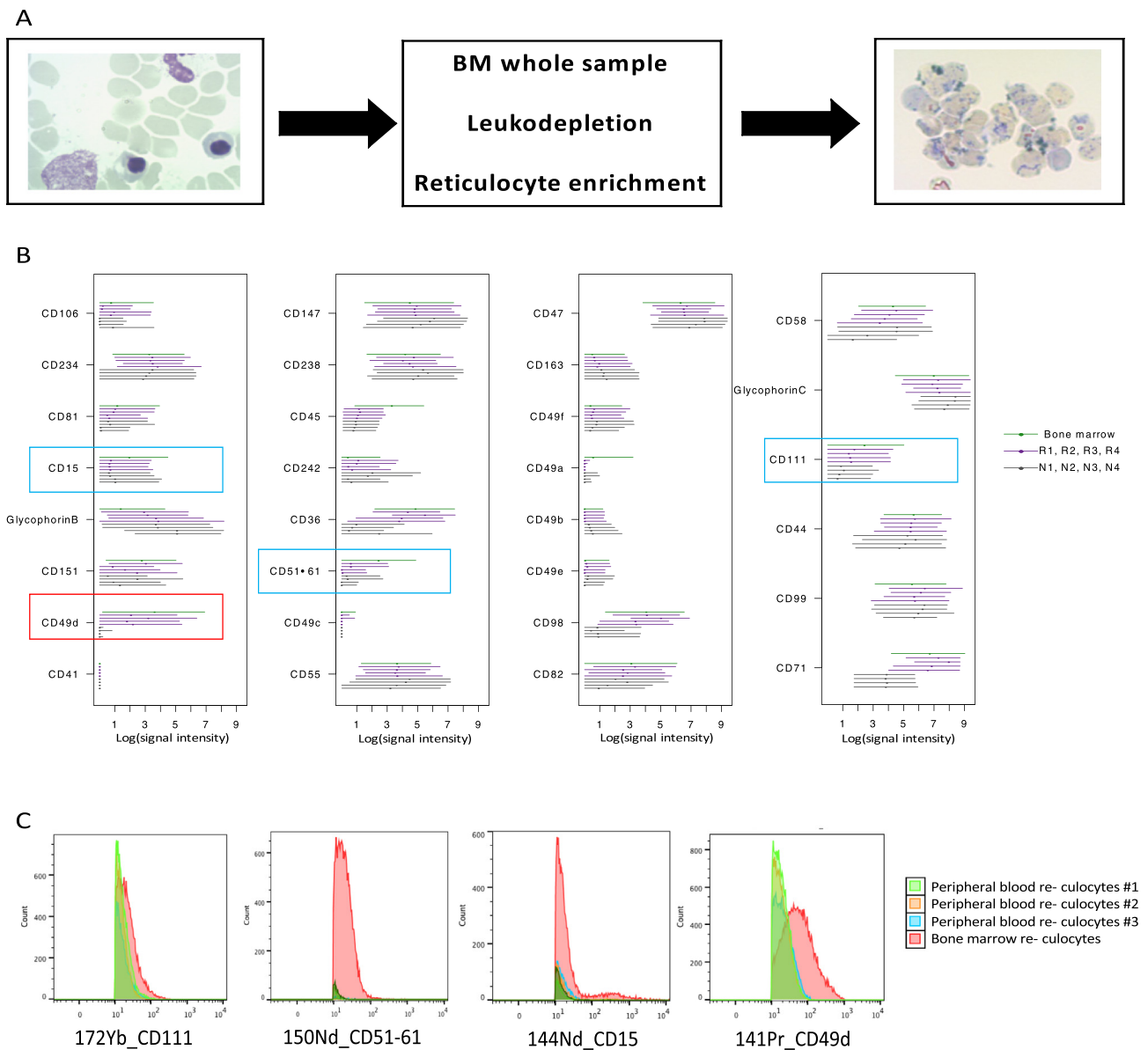


**Fig. 4.** Comparison of signal intensities (log scale) of all RBCs markers determined by CyTOF in peripheral blood vs bone marrow. (A) Preparation of bone marrow-derived reticulocytes for CyTOF analysis: whole bone marrow samples (Giemsa stained in left) carrying nucleated PBMCs where filtered and non-nucleated reticulocytes were then enriched using CD71 immune-magnetic labeling (NMB stained reticulocytes in right). (B) Differential markers intensity of mature RBCs Duffy<sup>+</sup> samples (N1–N4) and reticulocyte Duffy<sup>+</sup> samples (R1–R4) from peripheral blood compared to bone marrow-derived reticulocytes. Red box refers to the top differentially expressed marker intensity of CD49d; blue box for other markers differentially expressed in bone marrow. (C) Histogram with RBC markers highly expressed in bone marrow-derived reticulocytes compared to peripheral blood reticulocytes: CD111, CD51–61, CD15 and CD49d. (For interpretation of the references to color in this figure legend, the reader is referred to the web version of this article.)

$r > 0.8$ ). Among these fast disappearing markers, CD49d shows the fastest decrease in expression, being practically absent in mature RBCs. In contrast, some other markers (CD47, CD99, CD238, CD44, CD234, CD55, CD151, CD82 and CD58) show a smoother decreasing expression. These markers are also correlated among themselves in both reticulocyte and mature RBCs (Pearson's  $r > 0.8$ ) (Fig. 3B). To

demonstrate how mass cytometry substantially adds to the study of reticulocyte maturation, we performed a multidimensional analysis using Spanning-tree Progression Analysis of Density-normalized Events (SPADE) and interestingly noted that reticulocytes populations are heterogeneous (Fig. 3C).

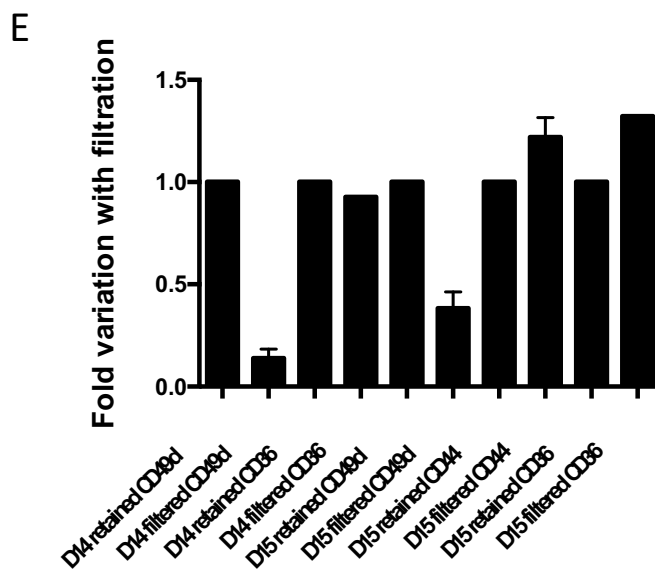
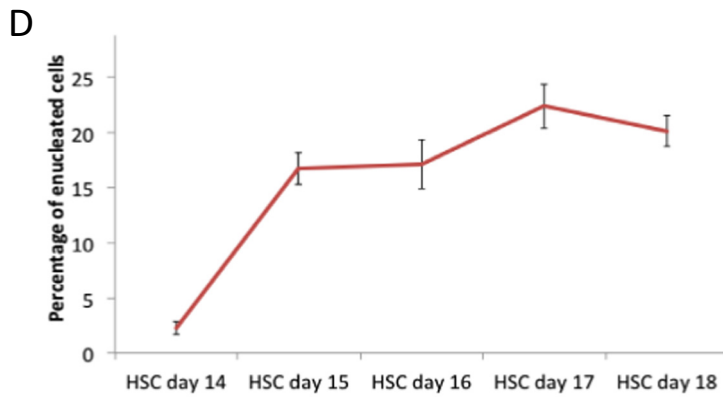
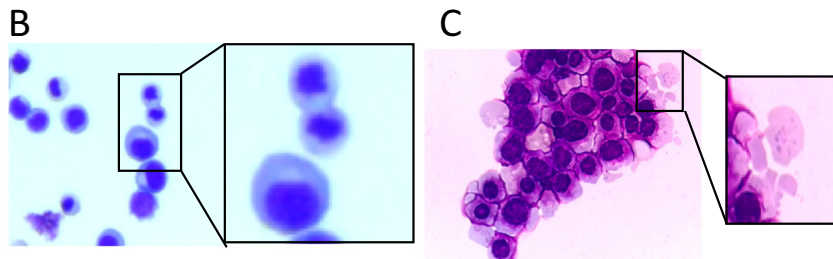
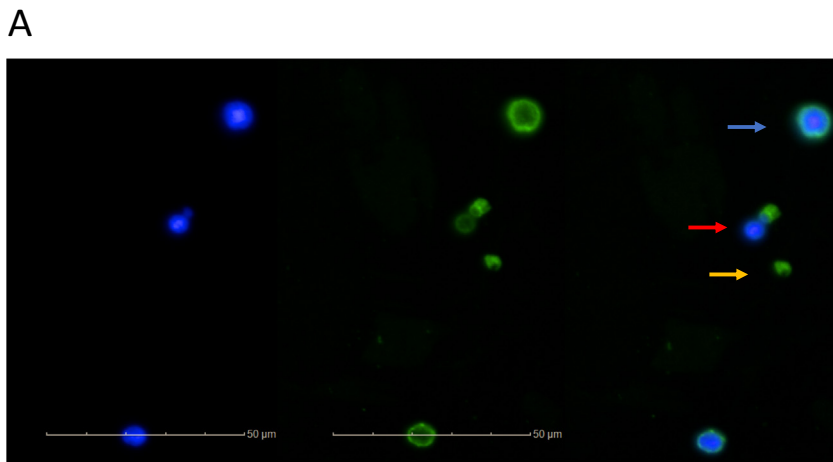


**Fig. 5.** Study on erythroblasts enucleation and CD49d expression loss in HSC cultures. (A) IFA image at day 15 showing a nucleated erythroblast with DAPI<sup>+</sup> nucleus (blue) and CD71-FITC<sup>+</sup> cytoplasm (green), enucleating erythroblast expelling its nucleus and a non-nucleated reticulocyte. (B–C) Giemsa-stained of a cytospin cell preparation showing nucleated and non-nucleated cells from HSC cultures at day 13 (A) and day 14 (B). (D) HSC cultures enucleation time-line: enucleation generally starts between day 14 and 15. (E) A histogram comparing the expression of CD49d before and after filtration at days 14 and 15 compared to the expression of CD36 and CD44 at day 15. (For interpretation of the references to color in this figure legend, the reader is referred to the web version of this article.)

### 3.4. Higher CD49d expression in bone marrow-derived reticulocytes

We extended our CyTOF analysis to the most immature reticulocytes hosted in the human bone marrow to further analyze the very initial steps of reticulocyte maturation. We selected bone marrow reticulocytes through an initial filtration step to get rid of nucleated WBCs as well as nucleated erythroid precursors; and by subsequent CD71 immune-magnetic labeling for reticulocyte enrichment (Fig. 4A). We obtained a similar phenotype as for peripheral circulation reticulocytes (Fig. 4B); yet, levels of CD15, CD51–61, CD111 and importantly for CD49d were clearly increased. This is consistent with an earlier developmental step of erythroid cells (Fig. 4C) and accounts for the lower level of CyTOF signal correlations of markers between R1–R4 compared to BM reticulocytes (Supplemental Fig. 3). We further confirm higher expression of CD49d in the more immature CD71<sup>hi</sup> FACS-sorted reticulocytes from peripheral blood by flow cytometric analysis (Supplemental Fig. 4) (as previously observed by CyTOF for reticulocytes with CD71 intensity > 400).

### 3.5. Dramatic changes in the expression of CD49d after erythroblast enucleation

To further demonstrate the fast disappearance pattern of CD49d, very early in reticulocyte maturation, we studied enucleation on erythroblasts (Fig. 5A–C) at different time points in several independent Hematopoietic Stem Cell (HSC) in vitro cultures (n = 8 for days 14, 15, 16 and 18 and n = 5 for day 17) (Fig. 5D). Through filtration, we separated nucleated HSC-cultured cells from non-nucleated ones at the peak enucleation on days 14 and 15 (Supplemental Fig. 5). We noted that CD49d expression promptly disappeared after enucleation (Fig. 5E). In contrast there were no changes or a slight increase in the expression of CD44 and CD36. Altogether, it re-enforces the expression pattern observed in our CyTOF results for bone marrow-derived reticulocytes. This indicates that CD49d is fast cleared after enucleation while other reticulocyte markers may be lost further ahead during the 40 h reticulocyte maturation in peripheral (as modeled in Supplemental Fig. 6).

### 3.6. Mitochondria content is lost at very early stages of reticulocyte maturation

Reticulocytes are known to contain remnants of organelles such as ribosomes, ER, Golgi apparatus and mitochondria. We have studied whether this mitochondrial content disappears progressively during maturation or in contrast it is restricted to the fast events occurring at the very early steps. We analyzed the mitochondrial content of different peripheral blood CD71-FACS-sorted populations of reticulocytes (CD71<sup>low</sup>, CD71<sup>med</sup> and CD71<sup>hi</sup>) by flow cytometry (Fig. 6A). Mitochondria content seemed to be exclusively present on very immature CD71<sup>hi</sup> reticulocytes in peripheral blood. We further explored the fast mitochondria clearance by employing a micro-engineered micro-well device (MWD) (Fig. 6B–C). A very conservative algorithm applied to the images that we obtained by High Content Imaging (HCI) (Fig. 6D–E) on different individual CD71 FACS-sorted population of cells confirmed that mitochondria is rapidly lost very early in reticulocyte maturation (Fig. 6F).

## 4. Discussion

Fully understanding the complex mechanism underlying the final stages of erythroid maturation remains of vital importance in many fields of study. Research on reticulocytes has become very important for the study of many hematologic diseases such as sickle cell disease [28]; and especially for hemotropic infectious diseases, with malaria being the most relevant [29–31]. Resolving the complexity of specific interactions mediating tropisms for each pathogens entry mechanism into

RBCs is of major importance [32, 33]. This may reveal new candidate targets to experimentally clarify invasion pathways in the case of *Plasmodium* species.

We have used and validated Mass Cytometry [34, 35] for the first time to capture the changes in surface complexity within single-cell RBC maturation and perform combinatorial expression and multi-dimensional analysis highlighting the heterogeneity of the reticulocyte population which deserves further insight. We have looked in depth into some markers hallmark of RBC immaturity. Of interest, CyTOF showed that CD49d, the leading hit of a cluster of fast disappearing reticulocyte markers, is more expressed in bone marrow-derived reticulocytes compared to peripheral blood; and within peripheral circulation uniquely in the most immature CD71<sup>hi</sup> reticulocytes (that, although in low quantity, were present in peripheral blood). Our data on a fast disappearance pattern of CD49d right after enucleation is syntonic with already published data on the most immature reticulocytes releasing exosomes bearing CD49d [36]. Interestingly these nano-vesicles are able to bind to fibronectin and vascular cells through CD49d [37], which promotes it as a promiscuous ligand to be studied in blood-borne diseases. Although interested on other heterodimeric members of the CD49 family (CD49a, CD49b, CD49c and CD49e), we could not provide additional insight; nonetheless, CD49a also showed higher levels of expression in the bone marrow.

Markers from the tetraspanins family CD151, CD81 and CD82 were also increasingly expressed in very immature reticulocytes from both, bone marrow and peripheral blood; yet, its lost is not as pronounced as for CD49d so to hold them responsible for specific young reticulocytes preferences [29, 30]. Nonetheless, tetraspanins are scaffold transmembrane proteins providing stability and molecular density [38]. Interestingly, CD82 and CD81 can be found co-localizing with CD49d in the surface of reticulocytes. Moreover, tetraspanin-enriched microdomains have been described as functional units in cell plasma membranes [39] and several studies have implicated their role on the entry of microbial pathogens [40–42], and of interest in HIV [43]. CD81 is also essential in the entry of rodent malaria parasites into hepatocytes [44]. Therefore, it seems reasonable that the involvement of CD49d, alone or together with tetraspanin microdomains, upon alternative invasion pathways or special tropisms of *P. vivax* for immature reticulocytes should be further investigated. Likewise, we show that mitochondria are preferentially found in very immature reticulocytes. Future mechanistic studies on the correlation of other RBC proteins with mitochondrial content should further serve as hypothesis generating. Yet, we speculate that mitochondria could aid buffering the increase of reactive oxygen species within reticulocyte generally happening after mitophagy, with its consequent damage in cellular components [16]. This may be beneficial for *P. vivax* progress within the sexual cycle once it has invaded its preferential target cell.

In summary, the state of the art phenotyping technology mass cytometry can be readily used for the in-depth characterization of the erythroid lineage both upstream and downstream of orthochromatic erythroblasts. Being able to apply this strong phenotyping technique to RBCs can broaden our understanding of the complex events taking place at different stages during erythropoiesis and can be useful to decipher special host tropisms, as well as a yet to be discovered specific receptor-ligand interactions, for *P. vivax* [45].

## Acknowledgements

Special thanks to the Flow Cytometry Core at the Morsani College of Medicine, University of South Florida. Very thankful to Jennifer Frahm, Colleen Urben and Greg Bauer from Fluidigm. Especially grateful to Michael Leipold from Human Immune Monitoring Center (HIMC), Stanford University and Wajeeh Saadi, University of South Florida.

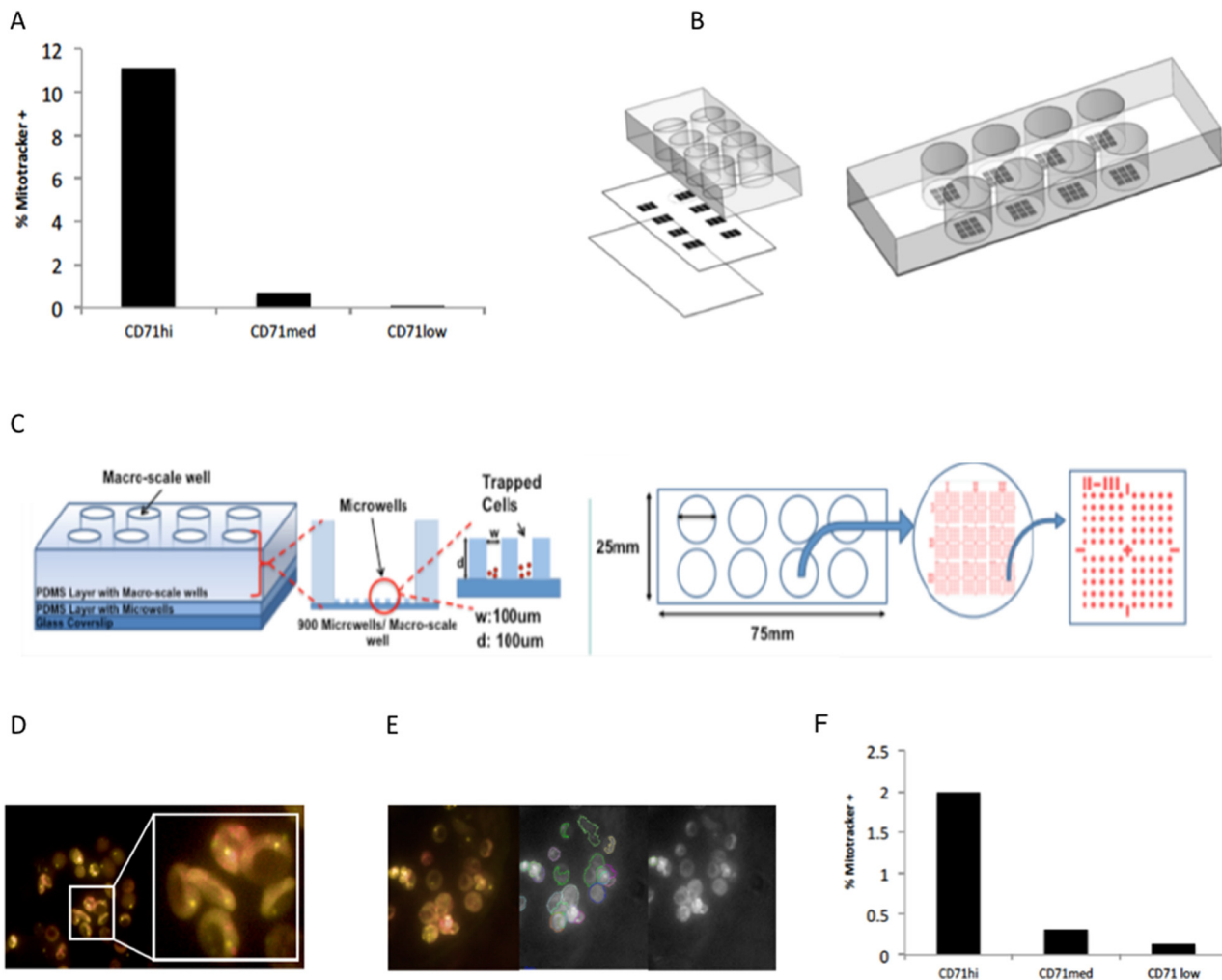


**Fig. 6.** Study on the mitochondria content of reticulocytes. (A) Histogram showing higher expression of Mitotracker in CD71<sup>hi</sup> FACS-sorted reticulocytes by flow cytometry compared to CD71<sup>med</sup> and CD71<sup>low</sup>. (B) Micro-Well Device (MWD) design and fabrication. (C) Images of CD71<sup>hi</sup> FACS-sorted reticulocytes stained with CD71-APC and Mitotracker Orange. (D) Selection the area to be image-analyzed by HCI using the Harmony Software (Perkin Elmer), identification of the number of cells in a single micro-well and application of a Mitotracker Orange-intensity based algorithm for determining the differential mitochondrial content of CD71<sup>hi</sup>, CD71<sup>med</sup> and CD71<sup>low</sup> reticulocytes (ratio spots > 2/spots > 0 of 1.99% for CD71<sup>hi</sup> cells, 0.30% for CD71<sup>med</sup> and 0.13% for CD71<sup>low</sup>). Cells were considered to be positive for mitochondria if there was at least two Mitotracker+ spots within the area previously identified as a cell and with intensity above a restrictive threshold previously established. (E) Histogram showing higher expression of Mitotracker in CD71<sup>hi</sup> reticulocytes based on the HCI analysis. (For interpretation of the references to color in this figure legend, the reader is referred to the web version of this article.)

## Funding

This work was supported by the Bill and Melinda Gates Foundation (grant number OPP1023643).

## Authorship contributions

RTL, SJB and JHA designed the experiments. RTL, SX, FBN, KS and AC performed the experiments. RTL, JHA, RHYJ, CQW, and SRA analyzed the data. RTL, CQW, SJB, JHA and RHJ wrote the manuscript. All authors read and approved the final manuscript.

## Competing interests

The authors declare that they have no competing interests.

## Appendix A. Supplementary data

Supplementary data to this article can be found online at <https://doi.org/10.1016/j.bcmd.2018.06.004>.

## References

- [1] M. Bessis, Erythroblastic island, functional unity of bone marrow, *Rev. Hematol.* 13 (1958) 8.
- [2] J.A. Chasis, N. Mohandas, Erythroblastic islands: niches for erythropoiesis, *Blood* 112 (2008) 470–478, <https://doi.org/10.1182/blood-2008-03-077883>.
- [3] C.B. Wölwer, L.B. Pase, H.B. Pearson, N.J. Gödde, K. Lackovic, D.C.S. Huang, S.M. Russell, P.O. Humbert, A chemical screening approach to identify novel key mediators of erythroid enucleation, *PLoS ONE* 10 (11) (2015) e0142655, <https://doi.org/10.1371/journal.pone.0142655>.
- [4] J. Hom, B.M. Dulmovits, N. Mohandas, L. Blanc, The erythroblastic island as an emerging paradigm in the anemia of inflammation, *Immunol. Res.* 63 (0) (2015) 75–89, <https://doi.org/10.1007/s12026-015-8697-2>.
- [5] G. Lee, A. Lo, S.A. Short, T.J. Mankelov, F. Spring, S.F. Parsons, K. Yazdanbakhsh, N. Mohandas, D.J. Anstee, J.A. Chasis, Targeted gene deletion demonstrates that the cell adhesion molecule ICAM-4 is critical for erythroblastic island formation, *Blood* 108 (6) (2006) 2064–2071, <https://doi.org/10.1182/blood-2006-03-006759>.
- [6] R.N. Jacobsen, A.C. Perkins, J.P. Levesque, Macrophages and regulation of erythropoiesis, *Curr. Opin. Hematol.* 22 (2015) 212–219, <https://doi.org/10.1097/MOH.0000000000000131>.
- [7] F.A. Spring, R.E. Griffiths, T.J. Mankelov, C. Agnew, S.F. Parsons, J.A. Chasis, D.J. Anstee, Tetraspanins CD81 and CD82 facilitate  $\alpha 4\beta 1$ -mediated adhesion of human erythroblasts to vascular cell adhesion molecule-1, *PLoS ONE* 8 (5) (2013) e62654, <https://doi.org/10.1371/journal.pone.0062654>.
- [8] D. Xu, Metabolic activation-related CD147-CD98 complex, *Mol. Cell. Proteomics* 4 (8) (2005) 1061–1071, <https://doi.org/10.1074/mcp.m400207-mcp200>.

- [9] J. Brittain, J. Han, K. Ataga, E. Orringer, L. Parise, Mechanism of CD47-induced  $\alpha 4 \beta 1$  integrin activation and adhesion in sickle reticulocytes, *J. Biol. Chem.* 279 (41) (2004) 42393–42402, <https://doi.org/10.1074/jbc.M407631200>.
- [10] B. Haynes, L. Hale, K. Patton, M. Martin, R. McCallum, Measurement of an adhesion molecule as an indicator of inflammatory disease activity: up-regulation of the receptor for hyaluronate (CD44) in rheumatoid arthritis, *Arthritis Rheum.* 34 (11) (2010) 1434–1443, <https://doi.org/10.1002/art.1780341115>.
- [11] A. Chow, M. Huggins, J. Ahmed, D. Hashimoto, D. Lucas, Y. Kunisaki, S. Pinho, M. Leboeuf, C. Noizat, N. van Rooijen, M. Tanaka, Z.J. Zhao, A. Bergman, M. Merad, P.S. Frenette, CD169<sup>+</sup> macrophages provide a niche promoting erythropoiesis under homeostasis, myeloablation and in JAK2V617F-induced polycythemia vera, *Nat. Med.* 19 (4) (2013) 429–436, <https://doi.org/10.1038/nm.3057>.
- [12] B. Fabrick, M. Polfiet, R. Vloet, R.C. van der Schors, A.J. Ligtenberg, L.K. Weaver, C. Geest, K. Matsuno, S.K. Moestrup, C.D. Dijkstra, T.K. van den Berg, The macrophage CD163 surface glycoprotein is an erythroblast adhesion receptor, *Blood* 109 (12) (2007) 5223–5229, <https://doi.org/10.1182/blood-2006-08-036467>.
- [13] X. An, N. Mohandas, Erythroblastic islands, terminal erythroid differentiation and reticulocyte maturation, *Int. J. Hematol.* 93 (2011) 139–143, <https://doi.org/10.1007/s12185-011-0779-x>.
- [14] B. Malleret, F. Xu, N. Mohandas, R. Suwanarusk, C. Chu, J.A. Leite, K. Low, C. Turner, K. Sriprawat, R. Zhang, O. Bertrand, Y. Colin, F.T.M. Costa, C.N. Ong, M.J. Ng, C.H. Lim, F. Nosten, L. Rénia, B. Russell, Significant biochemical, biophysical and metabolic diversity in circulating human cord blood reticulocytes, *PLoS ONE* 8 (10) (2013) e76062, <https://doi.org/10.1371/journal.pone.0076062>.
- [15] R.E. Griffiths, R.E. Griffiths, S. Kupzig, N. Cogan, T.J. Mankelov, V.M.S. Betin, K. Trakarnsanga, E.J. Massey, J.D. Lane, S.F. Parsons, D.J. Anstee, Maturing reticulocytes internalize plasma membrane in glycophorin A-containing vesicles that fuse with autophagosomes before exocytosis, *Blood* 119 (26) (2012) 6296–6306, <https://doi.org/10.1182/blood-2011-09-376475>.
- [16] J. Lee, S. Giordano, J. Zhang, Autophagy, mitochondria and oxidative stress: cross-talk and redox signalling, *Biochem. J.* 441 (2012) 523–540, <https://doi.org/10.1042/BJ20111451>.
- [17] M. Bessis, *Living Blood Cells and Their Ultrastructure*, (1973).
- [18] L. Heilmeyer, R. Westhäuser, Reifungsstadien an überlebenden reticulocyten in vitro und ihre bedeutung für die schaeetzung der täglichen haemoglobin-produktion in vivo, *Z. Klin. Med.* 121 (1932) 361.
- [19] H.C. Mel, M. Prenant, N. Mohandas, Reticulocyte motility and form: studies on maturation and classification, *Blood* 49 (1977) 1001–1009.
- [20] E.M. Pasini, M. Kirkegaard, P. Mortensen, H.U. Lutz, A.W. Thomas, M. Mann, In-depth analysis of the membrane and cytosolic proteome of red blood cells, *Blood* 108 (2006) 791–801, <https://doi.org/10.1182/blood-2005-11-007799>.
- [21] R.A. van Gestel, W.W. van Solinge, H.W. van der Toorn, G. Rijksen, A.J. Heck, R. van Wijk, M. Slijper, Quantitative erythrocyte membrane proteome analysis with Blue-native/SDS PAGE, *J. Proteome* 73 (2010) 456–465.
- [22] M.C. Wilson, K. Trakarnsanga, K.J. Heesom, N. Cogan, C. Green, A.M. Toye, S.F. Parsons, D.J. Anstee, J. Frayne, Comparison of the proteome of adult and cord erythroid cells, and changes in the proteome following reticulocyte maturation, *Mol. Cell. Proteomics* 15 (2016) 1938–1946, <https://doi.org/10.1074/mcp.M115.057315>.
- [23] S.C. Bendall, G.P. Nolan, M. Roederer, P.K. Chattopadhyay, A deep profiler's guide to cytometry, *Trends Immunol.* 33 (7) (2012) 323–332, <https://doi.org/10.1016/j.it.2012.02.010>.
- [24] D.R. Bandura, V.I. Baranov, O.I. Ornatsky, A. Antonov, R. Kinach, X. Lou, S. Pavlov, S. Vorobiev, J.E. Dick, S.D. Tanner, Mass cytometry: technique for real time single cell multitarget immunoassay based on inductively coupled plasma time-of-flight mass spectrometry, *Anal. Chem.* 81 (2009) 6813–6822, <https://doi.org/10.1021/ac901049w>.
- [25] A. Doerr, A flow cytometry revolution, *Nat. Methods* 8 (2011) 531–532.
- [26] H.E. Mei, M.D. Leipold, A.R. Schulz, C. Chester, H.T. Maecker, Barcoding of live human peripheral blood mononuclear cells for multiplexed mass cytometry, *J. Immunol.* 194 (2015) 2022–2031, <https://doi.org/10.4049/jimmunol.1402661>.
- [27] J.S. Cho, B. Russell, V. Kosasaivee, R. Zhang, Y. Colin, O. Bertrand, R. Chandramohanadas, C.S. Chu, F. Nosten, L. Renia, B. Malleret, Unambiguous determination of *Plasmodium vivax* reticulocyte invasion by flow cytometry, *Int. J. Parasitol.* 46 (2016) 31–39.
- [28] M.-C. Durpès, M.-D. Hardy-Dessources, W. El Nemer, J. Picot, N. Lemonne, J. Elion, M. Decastel, Activation state of  $\alpha 4 \beta 1$  integrin on sickle red blood cells is linked to the Duffy antigen receptor for chemokines (DARC) expression, *J. Biol. Chem.* 286 (2011) 3057–3064, <https://doi.org/10.1074/jbc.M110.173229>.
- [29] L. Martin-Jauler, A. Elizalde-Torrent, R. Thomson-Luque, M. Ferrer, J.C. Segovia, E. Herreros-Aviles, C. Fernández-Becerra, H.A. Del Portillo, Reticulocyte-prone malaria parasites predominantly invade CD71hi immature cells: implications for the development of an in vitro culture for *Plasmodium vivax*, *Malar. J.* 12 (1) (2013) 434, <https://doi.org/10.1186/1475-2875-12-434>.
- [30] B. Malleret, A. Li, R. Zhang, K.S.W. Tan, R. Suwanarusk, C. Claser, J.S. Cho, E.G. Koh, C.S. Chu, S. Pukrittayakamee, M.L. Ng, F. Ginhoux, L.G. Ng, C.T. Lim, F. Nosten, G. Snounou, L. Rénia, B. Russell, *Plasmodium vivax*: restricted tropism and rapid remodeling of CD71-positive reticulocytes, *Blood* 125 (2015) 1314–1324, <https://doi.org/10.1182/blood-2014-08-596015>.
- [31] J. Gruszczycy, U. Kanjee, L.J. Chan, S. Menant, B. Malleret, N.T.Y. Lim, C.Q. Schmidt, Y.F. Mok, K.M. Lin, R.D. Pearson, G. Rangel, B.J. Smith, M.J. Call, M.P. Weekes, M.D.W. Griffin, J.M. Murphy, J. Abraham, K. Sriprawat, M.J. Menezes, M.U. Ferreira, B. Russell, L. Renia, M.T. Duraisingh, W.H. Tham, Transferrin receptor 1 is a reticulocyte-specific receptor for *Plasmodium vivax*, *Science* 359 (2018) 48–55, <https://doi.org/10.1126/science.aan1078>.
- [32] J.G. Beeson, D.R. Drew, M.J. Boyle, G. Feng, F.J.I. Fowkes, J.S. Richards, Merozoite surface proteins in red blood cell invasion, immunity and vaccines against malaria, *FEMS Microbiol. Rev.* 40 (2016) 343–372, <https://doi.org/10.1093/femsre/fuw001>.
- [33] D.T. Riglar, D. Richard, D.W. Wilson, M.J. Boyle, C. Dekiwadia, L. Turnbull, F. Angrisano, D.S. Marapana, K.L. Rogers, C.B. Whitchurch, J.G. Beeson, A.F. Cowman, S.A. Ralph, J. Baum, Super-resolution dissection of coordinated events during malaria parasite invasion of the human erythrocyte, *Cell Host Microbe* 9 (2011) 9–20.
- [34] M.D. Leipold, E.W. Newell, H.T. Maecker, Multiparameter phenotyping of human PBMCs using mass cytometry, *Immunosenescence: Methods and Protocols*, 2015, pp. 81–95, [https://doi.org/10.1007/978-1-4939-2963-4\\_7](https://doi.org/10.1007/978-1-4939-2963-4_7).
- [35] S.C. Bendall, G.P. Nolan, From single cells to deep phenotypes in cancer, *Nat. Biotechnol.* 30 (2012) 639–647, <https://doi.org/10.1038/nbt.2283>.
- [36] C. Olver, M. Vidal, Proteomic analysis of secreted exosomes, *Subcellular Proteomics*, 2007, pp. 99–131.
- [37] S. Rieu, C. Géminard, H. Rabesandratana, J. Sainte-Marie, M. Vidal, Exosomes released during reticulocyte maturation bind to fibronectin via integrin  $\alpha 4 \beta 1$ , *Eur. J. Biochem.* 267 (2000) 583–590.
- [38] C.M. Termini, M.L. Cotter, K.D. Marjon, T. Buranda, K.A. Lidke, J.M. Gillette, et al., The membrane scaffold CD82 regulates cell adhesion by altering  $\alpha 4$  integrin stability and molecular density, *Mol. Biol. Cell* 25 (2014) 1560–1573, <https://doi.org/10.1091/mbc.E13-11-0660>.
- [39] M. Yáñez-Mó, O. Barreiro, M. Gordon-Alonso, M. Sala-Valdés, F. Sánchez-Madrid, Tetraspanin-enriched microdomains: a functional unit in cell plasma membranes, *Trends Cell Biol.* 19 (2009) 434–446, <https://doi.org/10.1016/j.tcb.2009.06.004>.
- [40] S. Charrin, S. Jouannet, C. Boucheix, E. Rubinstein, Tetraspanins at a glance, *J. Cell Sci.* 127 (2014) 3641–3648, <https://doi.org/10.1242/jcs.154906>.
- [41] J. He, E. Sun, M.V. Bujny, D. Kim, M.W. Davidson, X. Zhuang, Dual function of CD81 in influenza virus uncoating and budding, *PLoS Pathog.* 9 (10) (2013), <https://doi.org/10.1371/journal.ppat.1003701>.
- [42] K.D. Scheffer, A. Gawlitza, G.A. Spoden, X.A. Zhang, C. Lambert, F. Berditchevski, L. Florin, Tetraspanin CD151 mediates papillomavirus type 16 endocytosis, *J. Virol.* 87 (2013) 3435–3446, <https://doi.org/10.1128/JVI.12906-12>.
- [43] D.N. Kremenstov, P. Rassam, E. Margeat, N.H. Roy, J. Schneider-Schaulies, P.E. Milhiet, M. Thali, HIV-1 assembly differentially alters dynamics and partitioning of tetraspanins and raft components, *Traffic* 11 (2010) 1401–1414.
- [44] L. Foquet, C.C. Hermesen, L. Verhoye, G.J. van Gemert, R. Cortese, A. Nicosia, R.W. Sauerwein, G. Leroux-Roels, P. Meuleman, Anti-CD81 but not anti-SR-BI blocks *Plasmodium falciparum* liver infection in a humanized mouse model, *J. Antimicrob. Chemother.* 70 (6) (2015) 1784–1787, <https://doi.org/10.1093/jac/dkx019>.
- [45] F.B. Ntumngia, R. Thomson-Luque, Lde.M. Torres, K. Gunalan, L.H. Carvalho, J.H. Adams, A novel erythrocyte binding protein of *Plasmodium vivax* suggests an alternate invasion pathway into Duffy-positive reticulocytes, *MBio* 7 (4) (2016), <https://doi.org/10.1128/mBio.01261-16>.